Organic Electronics 11 (2010) 820–830

Contents lists available at ScienceDirect

Organic Electronics

journal homepage: www.elsevier.com/locate/orgel

Organic thin-film transistor properties and the structural relationships between various aromatic end-capped triisopropylsilylethynyl anthracene derivatives

Jong-Hwa Park [a], Dong Hoon Lee [b], Hoyoul Kong [a], Moo-Jin Park [c], In Hwan Jung [a], Chan Eon Park [b,*], Hong-Ku Shim [a,*]

[a] Department of Chemistry, Korea Advanced Institute of Science and Technology, Guseong-Dong, Yuseong-Gu, Daejeon 305-701, Republic of Korea
[b] Department of Chemical Engineering, Pohang University of Science and Technology, Hyoja-Dong, Nam-Gu, Pohang, Gyungbuk 790-784, Republic of Korea
[c] Polymer Science and Engineering Program, Korea Advanced Institute of Science and Technology, Guseong-Dong, Yuseong-Gu, Daejeon 305-701, Republic of Korea

ARTICLE INFO

Article history:
Received 23 November 2009
Received in revised form 15 January 2010
Accepted 28 January 2010
Available online 4 February 2010

Keywords:
Organic thin-film transistor
Anthracene
Charge-carrier mobility

ABSTRACT

We describe the preparation and characterization of single crystals and thin films composed of three new small molecules based on soluble triisopropylsilylethynyl (*TIPS*)-substituted anthracene (*TIPSAnt*) for use in organic thin-film transistors (TFTs); the three molecules examined were *TIPSAnt* derivatives containing thiophene (*TIPSAntT*), benzothiophene (*TIPSAntBeT*), or phenyl thiophene (*TIPSAntPT*) end cappers. We elucidated the relationship between the molecular structures and TFT performances by measuring the thermal, optical, electrochemical, crystalline, and morphological properties of these molecules. *TIPSAntPT* was able to achieve a "bricklayer" type of molecular stacking structure, facilitated by the bulky phenyl thiophene substituents. This is the first report of a "bricklayer" stacking structure of triisopropylsilylethynyl anthracene derivatives. Among the three molecules, *TIPSAntPT* showed the highest TFT mobility, 0.063 cm^2/Vs for the film state and 0.12 cm^2/Vs for single crystals. By contrast, in the case of in *TIPSAntBeT*, the introduction of the rigid substituent group led to poor TFT device performance. TFT device performances could be explained in terms of thin-film morphology, investigated by atomic force microscopy (AFM) and X-ray diffraction (XRD) analysis.

1. Introduction

Many classes of π-conjugated organic small molecules and polymers have been developed into semiconductors for organic thin-film transistors (OTFTs) over the past several decades [1–3]. Recently, interest in solution-processable materials that enable inexpensive device fabrication has increased, and remarkable achievements have been reported [4]. By using simple solution techniques, such as spin-coating, drop-casting, or inkjet-printing, OTFTs can be fabricated at prices that are comparable to conventional inorganic transistors [5,6].

Apart from polymer-based OTFTs, a variety of small molecule OTFTs have been reported to be solution-processable. Among these, triisopropylsilylethynyl (*TIPS*)-substituted pentacene derivatives are considered to be most promising candidates [7,8]. Anthony et al. developed the *TIPS*-pentacene system by introducing bulky *TIPS* groups into highly crystalline, insoluble, and unstable pentacene at the peri position, and, surprisingly, the bulky groups improved not only the solubility and stability, but also the crystallinity of the molecules [9]. The single crystals packed in either a "bricklayer" structure (each molecule engaged in π-overlap with two adjacent molecules) or a "slipped-stacked" structure (each molecule engaged in π-overlap with only one adjacent molecule), depending on the relative bulkiness of the substituents of the silylethynyl group with respect to the length of the conjugated

* Corresponding authors.
E-mail addresses: cep@postech.ac.kr (C.E. Park), hkshim@kaist.ac.kr (H.-K. Shim).

1566-1199/$ - see front matter © 2010 Elsevier B.V. All rights reserved.
doi:10.1016/j.orgel.2010.01.024

core [9]. It was found that the "bricklayer" structure showed much better TFT performance than the "slipped-stacked" structure, and that the bulkiness of the substituents (relative to the molecular size) which produced the bricklayer structure was required to fall within a narrow range; If the size of the substituents was too large or too small, a "slipped-stacked" or "herringbone" structure occurred, which showed poorer TFT performance. Based on this strategy, many small molecules yielding promising TFT performances have been developed [10–12].

In 2007, our group reported the development of promising *TIPS* anthracene derivatives (*TIPSAnts*) using the anthracene moiety in place of pentacene [13]. Anthracene is much more stable with respect to Diels–Alder reactions, and this stability prevents butterfly dimer decomposition, improves processability, and yields high crystallinity [14–16]. Small molecules containing *TIPSAnt* showed promising optical, electrochemical, and crystalline properties that resulted in moderate charge-carrier mobilities. However, to achieve higher TFT performances, further improvements were required. Because *TIPSAnt* contains dibromo moieties, it can serve as a soluble oligomer core for aromatic coupling reactions. The synthetic functionalities of *TIPSAnt* led to the development of a variety of new *TIPSAnt*-based small molecules.

Recently, we reported single crystal TFT performances of *TIPSAnt* derivatives by incorporating naphthalene and bithiophene moieties as counterparts of *TIPSAnt* [17]. Device performance was increased by increasing the molecular surface area available for π-stacking overlap. However, *TIPSAntNa* and *TIPSAntBT* single crystals showed only a "slipped-stacked" structure.

In this paper, we report three new small molecules based on *TIPSAnt*, 2,6-bis(thiophene-2′-yl)-9,10-bis(triisopropylsilylethynyl)anthracene (*TIPSAntT*), 2,6-bis(benzo[b]thiophene-2′-yl)-9,10-bis(triisopropylsilylethynyl)anthracene (*TIPSAntBeT*), and 2,6-bis(5′-phenyl-thiophene-2′-yl)-9,10-bis(triisopropylsilylethynyl)anthracene (*TIPSAntPT*). We systematically designed these new small molecules to elucidate the relationship between thin-film structure and TFT device performance for aromatic end-capped *TIPSAnt* derivatives. Thiophene, benzothiophene, and phenyl thiophene were used as end cappers for the *TIPSAnt* series. Two structural factors were considered: (1) the increase in the rigidity caused by fusing the aromatic rings, and (2) the increase in the effective π-stacking area of the "bricklayer" structure. We performed a comparative study to investigate the relationship between the molecular structures and TFT performances by measuring the thermal, optical, electrochemical, crystalline, and morphological properties of these molecules. This study demonstrated, for the first time, that the preparation of a "bricklayer" stacking structure using a *TIPSAnt* derivative yields high TFT performance.

2. Experimental

2.1. Instruments and reagents

^{1}H and ^{13}C NMR spectra were recorded on a Bruker AVANCE 400 spectrometer with tetramethylsilane as an internal reference. For the NMR measurements, chloroform-d ($CDCl_3$) was used as the solvent for the materials except *TIPSAntBeT* (1,1,2,2,-tetrachloroethane-d_2). Elemental analysis was performed using EA-1110-FISONS elemental analyzer. UV–vis spectra were measured by using a Jasco V-530 UV/vis Spectrometer. Thermogravimetric analysis (TGA) measurement was performed under nitrogen atmosphere at a heating rate of 10 °C/min using TA Q500 instrument, and the differential scanning calorimetric (DSC) measurement was made using TA Q100 instrument operated under nitrogen atmosphere. Cyclic voltammetry (CV) measurement was performed on an AUTOLAB/PGSTAT12 at room temperature with a three-electrode cell in a solution of 0.1 M tetrabutylammonium tetrafluoroborate (TBABF4) in anhydrous acetonitrile at room temperature under nitrogen gas with a scan rate of 50 mV/s. The working electrode was the oligomer coated platinum, the counter electrode was a platinum wire, and the reference electrode was $Ag/AgNO_3$ (0.10 M) which was separated by a diaphragm. The measurements were calibrated using ferrocene as a standard. The single crystal for X-ray analysis was typically grown from hexane and chlorobenzene. Analyses were performed on a Bruker SMART Apex II X-ray Diffractometer. Data have been submitted as .cif files. AFM (Multimode IIIa, Digital Instruments) operating in tapping-mode was used to image surface morphology of our semiconductor. Synchrotron X-ray diffraction analyses of PAT4 films were performed at the 10C1 beam line (wavelength ≈1.54 Å) of the Pohang Accelerator Laboratory (PAL). Top-contact OTFTs were fabricated on a common gate of highly n-doped silicon with a 300 nm thick thermally grown SiO_2 dielectric layer. Substrates were modified with octyltrichlorosilane from a toluene solution for 2 h at room temperature. Films of organic semiconductor were spin-coated at 2000 rpm from 0.7 wt.% chloroform or chlorobenzene solution, with nominal thickness 45 nm. Gold source and drain electrodes were evaporated on the top of semiconductor (100 nm). For all measurements, we used channel lengths (L) of 150 μm and channel widths (W) of 1500 μm. Electrical characteristics of the TFTs were measured in air using both Keithley 236 source/measure units. The carrier mobility was calculated in the saturation regime from the slope of a plot of the square root of the drain current versus gate voltage (V_G) by fitting the data to the following equation: $I_{DS} = (WC_i/2L)\mu(V_G - V_T)^2$, where I_{DS} is the drain current, μ is the carrier mobility and V_T is the threshold voltage. For single crystal TFTs, saturated chlorobenzene solution of the small molecules was slowly evaporated at room temperature on OTS-modified SiO_2 substrates. After 1 or 2 days, well-defined rod-type single crystals were obtained and gold electrode was patterned onto the single crystals by thermal evaporation with thickness of 100 nm. Width and length of the channels were calculated from optical microscopy (OM) images. The thickness of single crystals was measured using an alpha stepper (Alpah Step 500, Tencor).

Chemical reagents were purchased from Aldrich Chemical Co. and were used without further purification. Solvents with analytical-grade were used during the whole experiments, and all chemicals were used without further purification. 2,6-Dibromo-9,10-bis-(triisopropylsilylethy-

nyl)anthracene (*TIPSAnt*) [13], 2-pinacolborylthiophene (1a) [18], and 2-(4′,4′,5′,5′-tetramethyl-1′,3′,2′-dioxaborolane)benzo[b]thiophene (1b) [19], 5-phenyl-1-tributyl stannyl thiophene (1c) [20] were synthesized according to the reported procedures.

2.2. Synthesis

2.2.1. Synthesis of 2,6-Bis(thiophene-2′-yl)-9,10-bis(triisopropylsilylethynyl)anthracene (TIPSAntT)

Into 150 mL two-neck flask were added *TIPSAnt* (1 g, 1.43 mmol) and 2-pinacolborylthiophene (1a) (0.66 g, 3.16 mmol) in 15 mL of anhydrous toluene. Catalytic amount of tetrakis(triphenyl phosphine)palladium(0) was transferred into the mixture in dry box. Subsequently, (2 M Na_2CO_3) sodium carbonate (0.76 g, 7.21 mmol) deaerated for 30 min and the phase transfer catalyst, Aliquat®336 (0.29 g, 0.72 mmol) in toluene purged under nitrogen for 1 h was transferred via cannula. The reaction mixture was stirred at 90 °C for 3 days and cooled to room temperature. Then, the reaction mixture was poured into saturated sodium bicarbonate solution and extracted with EA. The organic layer was washed with brine, and then dried over anhydrous $MgSO_4$. The crude product was column chromatographed with hexane and MC mixture as the eluent, and then crystallized from hexane and MC to yield *TIPSAntT* (0.72 g, 71.0%) as bright orange crystal. ^{1}H NMR ($CDCl_3$, ppm) δ = 8.84 (d, 2H), 8.60 (d, 2H), 7.87 (dd, 2H), 7.53 (d, 2H), 7.37 (d, 2H), 7.14 (dd, 2H), 1.31 (m, 42H). ^{13}C NMR ($CDCl_3$, ppm) δ = 144.31, 132.57, 132.49, 132.19, 128.25, 127.92, 125.79, 125.72, 123.99, 122.97, 118.53, 105.28, 103.10, 19.00, 11.55. Anal. calcd for $C_{44}H_{54}S_2Si_2$: C, 75.15%; H, 7.74%; S, 9.12%. Found: C, 74.73%; H, 7.58%; S, 8.99%.

2.2.2. Synthesis of 2,6-bis(benzo[b]thiophene-2′-yl)-9,10-bis(triisopropylsilylethynyl)anthracene (TIPSAntBeT)

Into 150 mL two-neck flask were added *TIPSAnt* (1 g, 1.43 mmol) and 2-(4′,4′,5′,5′-tetramethyl-1′,3′,2′-dioxaborolane)benzo[b] thiophene (1b) (0.86 g, 3.31 mmol) in 20 mL of anhydrous toluene. Catalytic amount of tetrakis(triphenyl phosphine)palladium(0) was transferred into the mixture in dry box. Subsequently, (2 M Na_2CO_3) sodium carbonate (0.76 g, 7.21 mmol) deaerated for 30 min and the phase transfer catalyst, Aliquat®336 (0.29 g, 0.72 mmol) in toluene purged under nitrogen for 1 h was transferred via cannula. The reaction mixture was stirred at 90 °C for 3 days and cooled to room temperature. Then, the reaction mixture was poured into saturated sodium bicarbonate solution and extracted with MC. The organic layer was washed with brine, and then dried over anhydrous $MgSO_4$. The crude product was column chromatographed with hexane and MC mixture as the eluent, and then crystallized from chlorobenzene to yield *TIPSAntBeT* (0.63 g, 55.1%) as bright orange crystal. ^{1}H NMR (1,1,2,2-tetrachloroethane-d_2 at 100 °C, ppm) δ = 9.06 (s, 2H), 8.74 (d, 2H), 8.05 (d, 2H), 7.93 (d, 2H), 7.86 (d, 2H), 7.83 (s, 2H), 7.41 (m, 4H), 1.44 (m, 42H). ^{13}C NMR (1,1,2,2-tetrachloroethane-d_2 at 100 °C, ppm) δ = 144.34, 141.05, 140.35, 133.07, 132.98, 132.83, 128.25, 126.00, 124.85, 124.84, 124.77, 123.89, 122.46, 121.02, 119.35, 106.50, 103.41, 19.10, 12.01. Anal. calcd for $C_{52}H_{58}S_2Si_2$: C, 77.75%; H, 7.28%; S, 7.98%. Found: C, 77.24%; H, 7.02%; S, 7.68%.

2.2.3. Synthesis of 2,6-bis(5′-phenyl-thiophene-2′-yl)-9,10-bis(triisopropylsilylethynyl)anthracene (TIPSAntPT)

To a 150 mL two neck round-bottom flask equipped with a stir bar under N_2 was added *TIPSAnt* (0.60 g, 0.86 mmol) and 5-phenyl-1-tributylstannyl thiophene (1c) (1.16 g, 2.58 mmol). Tris(dibenzylideneacetone)dipalladium (0.016 g, 0.017 mmol) and tri-o-tolyphosphine (0.021 g, 0.069 mol) was transferred into the mixture in dry box. Subsequently anhydrous toluene (20 mL) was added and purged under nitrogen for 30 min. The reaction mixture was stirred at 120 °C for 3 days and cooled to room temperature. Then, solvent was evaporated with rotary evaporator and dried at vacuum. The crude product was column chromatographed with hexane and MC mixture as the eluent, and then crystallized from hexane and chlorobenzene to yield *TIPSAntPT* (0.56 g, 75.7%) as bright orange crystal. ^{1}H NMR ($CDCl_3$, ppm) δ = 8.86 (d, 2H), 8.59 (d, 2H), 7.91 (dd, 2H), 7.66 (dd, 4H), 7.49 (d, 2H), 7.41 (t, 4H), 7.35 (d, 2H), 7.30 (t, 2H), 1.32 (m, 42H). ^{13}C NMR ($CDCl_3$, ppm) δ = 144.39, 143.44, 134.24, 132.60, 132.35, 132.22, 128.99, 127.90, 127.67, 125.58, 125.28, 124.94, 124.23, 122.79, 118.51, 105.29, 103.13, 19.04, 11.61. Anal. calcd for $C_{56}H_{62}S_2Si_2$: C, 78.63%; H, 7.31%; S, 7.50%. Found: C, 78.52%; H, 7.28%; S, 7.52%.

3. Results and discussion

3.1. Synthesis of the small molecules

The soluble oligomer core, *TIPSAnt*, was synthesized according to procedures developed previously [13]. The bromo groups of *TIPSAnt* enabled coupling of the molecules to a variety of borolanylaryl or stannylaryl molecules, for example, acene, thiophene, or fluorene derivatives. In the present work, we chose thiophene, benzothiophene, and phenyl thiophene for *TIPSAntT*, *TIPSAntBeT*, and *TIPSAntPT*, respectively, as counterparts of *TIPSAnt*. Aromatic end cappers (1a–1c) were easily synthesized via well-known lithiation methods. *TIPSAntT* and *TIPSAntBeT* were synthesized via a Suzuki coupling reaction, and *TIPSAntPT* was synthesized via a Stille coupling reaction with high yields, as shown in Scheme 1. To achieve high purity, we purified the molecules by column chromatography, followed by several consecutive recrystallizations. The products were bright orange highly crystalline solids. The relative solubilities of the resulting products were as follows: *TIPSAntT* > *TIPSAntPT* > *TIPSAntBeT*. *TIPSAntT* showed good solubility in common organic solvents, such as THF, toluene, and chloroform, whereas *TIPSAntBeT* was soluble only in hot chlorobenzene. *TIPS* groups improved the solubility of the π-conjugated rings, but as the molecular size and rigidity increased, the solubility of the molecules decreased. The compounds were characterized by ^{1}H NMR, ^{13}C NMR, and elemental analysis.

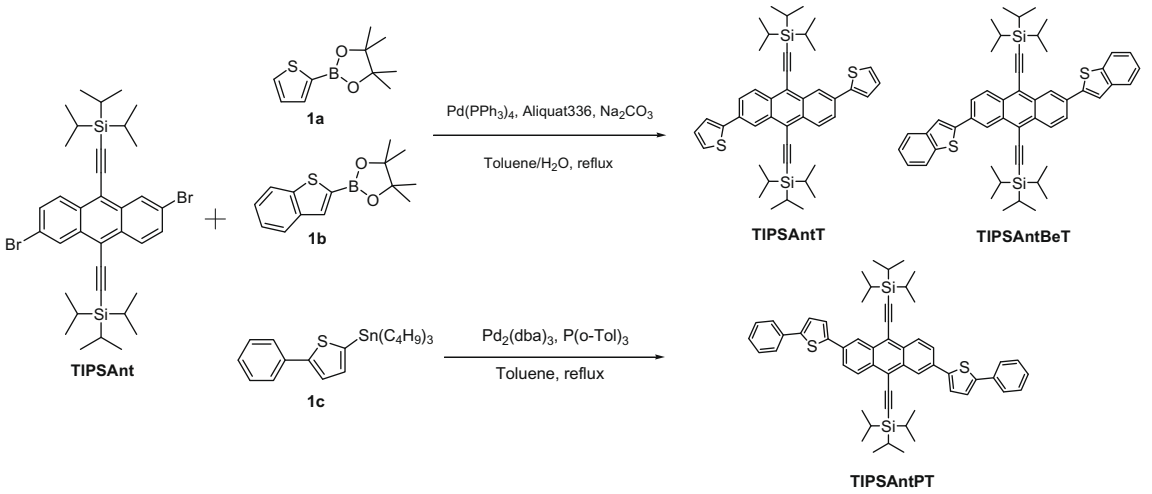

Scheme 1. Syntheses of the small molecules.

3.2. Thermal properties

The thermal stabilities of the small molecules were characterized by thermogravimetric analysis (TGA) under a nitrogen atmosphere. *TIPSAntT* exhibited good thermal stability, with a decomposition temperature, based on 5% weight loss (T_{d5}), of 355 °C, whereas *TIPSAntBeT* and *TIPSAntPT* exhibited excellent thermal stabilities, showing a T_{d5} of 416° and 420 °C, respectively. The larger molecular weights of *TIPSAntBeT* and *TIPSAntPT* may have contributed to their improved thermal stabilities. The thermal transitions of the small molecules were studied by differential scanning calorimetry (DSC) under a nitrogen atmosphere. *TIPSAntT* exhibited liquid crystalline properties, with the first endothermal peak at 173 °C and the second endothermal peak at 290 °C, and corresponding exothermal peaks at 140 °C and 220 °C. *TIPSAntBeT* and *TIPSAntPT* exhibited similar transition behavior, with major melting endotherms at 209 and 304 °C, and corresponding crystallization exotherms upon cooling at 206 and 262 °C. All peaks were significant and reversible, without the presence of additional thermal transitions. From these thermal responses, we concluded that the small molecules were highly crystalline and should form well-ordered thin films when deposited onto a substrate. DSC results are shown in Fig. 1.

3.3. Optical properties

The UV–vis absorption spectra of the small molecules were recorded both in solution (chlorobenzene) and in film states, as shown in Fig. 2. The UV–vis data for the small molecules is summarized in Table 1. All small molecules showed good absorption properties, with vibronic structures in both solution and film states. In both the solution and film states, the absorption spectra of the small molecules showed relative red-shifts as follows: *TIPSAntT* < *TIPSAntBeT* < *TIPSAntPT*. The largest red-shift in the absorption spectrum of *TIPSAntPT* suggested the presence of increasing electron delocalization along the main chain due to more extensive conjugation. The lowest energy transitions in the film states were more red-shifted (18–37 nm) than those in solution states for all small molecules (see Δ2nd Max in Table 1). The intensities of the lowest energy transitions were also larger in the film states compared to the intensities in the solution states. The red-shifts and increased intensities demonstrated extended π-conjugation and substantially more intermolecular ordering within the 2D stacking of the small molecules in the film state. The most striking red-shift, observed for *TIPSAntPT* (37 nm), indicated that this molecule has the strongest intermolecular interactions. The existence of strong interactions between the π-conjugated systems of neighboring molecules in the solid state is desirable for good TFT device performance.

3.4. Electrochemical properties

To investigate the electrochemical stability and the charge transport properties of the small molecules, we carried out cyclic voltammetry (CV) measurements on thin films of the small molecules, summarized in Table 2. The small molecules showed reversible waves for both p-doping and n-doping processes. The oxidation potentials E_{ox} (p-doping) for *TIPSAntT*, *TIPSAntBeT*, and *TIPSAntPT* were 0.99, 1.13, and 0.96 V, respectively. The relatively high oxidation potentials for *TIPSAnts*, compared to *TIPS* pentacene (380 mV), [21] resulted in better oxidation stability of the materials. The highest occupied molecular orbital (HOMO) levels of *TIPSAntT*, *TIPSAntBeT*, and *TIPSAntPT* were estimated to be −5.39, −5.53, and −5.36 eV, respectively, using the previously reported empirical equation [22]. The observation that *TIPSAntBeT* had the lowest HOMO was attributed to reduced delocalization along the backbone through the introduction of a fused aromatic unit, benzothiophene. The delocalization of electrons from the benzothiophene unit onto the backbone was less favorable than from a single thiophene and benzene ring, due to the larger resonance stabilization energy of the fused ring [23]. It is worth noting that among the three materials, the

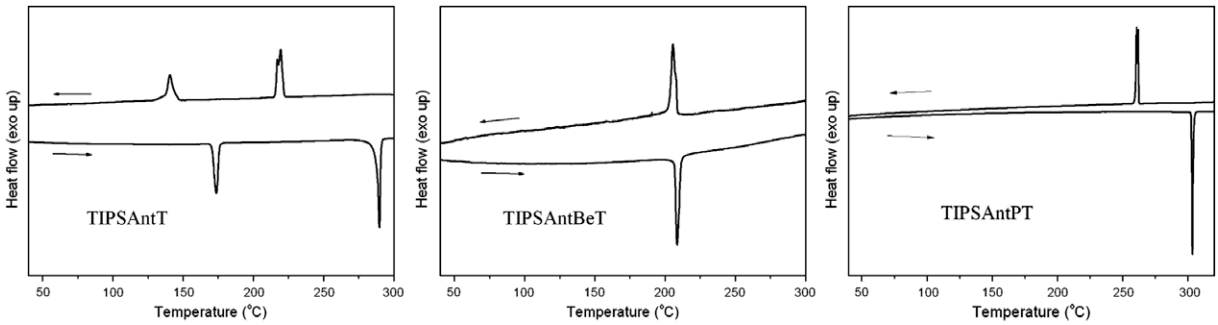

Fig. 1. DSC scans of the small molecules.

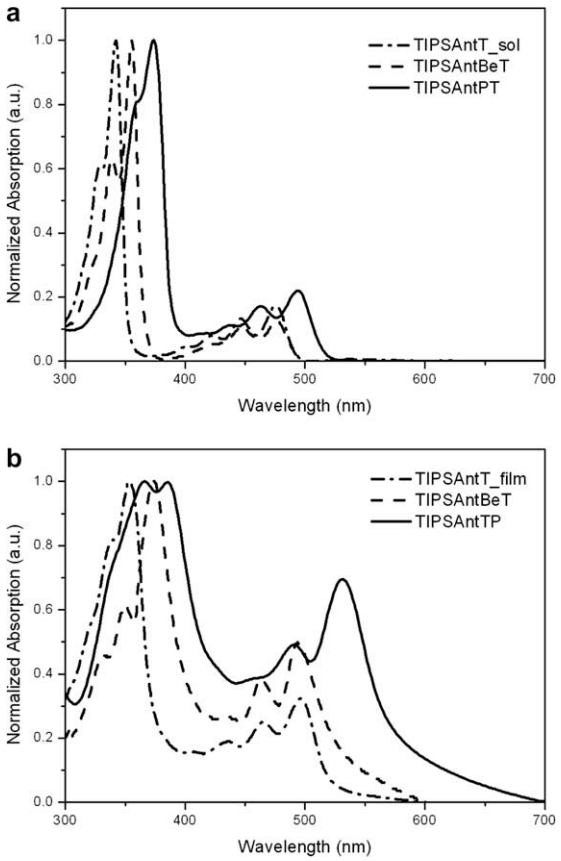

Fig. 2. UV–vis absorption of the small molecules. (a) In a chlorobenzene solution (b) in the spin-coated film state.

HOMO level of *TIPSAntPT* provided the best match to the work function of gold metal [24]. As a result, hole injection from the gold source electrode in p-type thin-film transistors composed of *TIPSAntPT* was expected to be the most efficient among the three materials. In contrast, the lowest lying HOMO level of *TIPSAntBeT* would be expected to increase the hole injection barrier between the gold electrodes and the *TIPSAntBeT* film. The relative band gaps of *TIPSAnts*, calculated from CV measurements and the onset of absorption in the film states, decreased in the order *TIPSAntT* > *TIPSAntBeT* > *TIPSAntPT*, as summarized in Table 2.

Table 1
UV–vis absorption properties of the small molecules.

λ_{max}	UV_sol[a]	UV_film[b]	Δ1st Max[c]	Δ2nd Max[d]
TIPSAntT	342, 475	353, 496	11	21
TIPSAntBeT	357, 476	373, 494	16	18
TIPSAntPT	373, 494	366, 531	−7	37

[a] In chlorobenzene solution.
[b] Spin-coated thin film from chlorobenzene solution.
[c] The 1st maximum peak difference between solution and film states around 340–370 nm.
[d] The 2nd maximum peak difference between solution and film states around 470–530 nm.

The low band gap of *TIPSAntPT* was attributed to the extended conjugation system of the material, which benefited from the long conjugation length of the main chain, as described in Section 3.3.

3.5. X-ray crystallography

Crystallographic analysis allows for the rapid screening of potential OTFT materials. Single crystals of small molecules, easily grown from hexane and chlorobenzene, were analyzed by X-ray crystallography.

Fig. 3 shows the π-stacking structures of the small molecules in single crystals. All of the molecules showed face-to face molecular interactions similar to our previous results [13]. The interplanar distances in the three molecules were almost identical: 3.54, 3.55, and 3.54 Å for *TIPSAntT*, *TIPSAntBeT*, and *TIPSAntPT*, respectively. Single crystals of *TIPSAntT* and *TIPSAntBeT* showed "slipped-stacked" structures similar to that previously reported for *TIPSAnts* [13,17], as shown in Fig. 3b and d. However, single crystals of *TIPSAntPT* showed a "bricklayer" structure, as shown in Fig. 3f. How the *TIPSAnt* columns interdigitate determines whether a "slipped-stacked" or "bricklayer" structure is formed. When *TIPSAntT* of *TIPSAntBeT* columns packed together, each conjugated core in one column adjoined two TIPS groups in an adjacent column to form a "slipped-stacked" structure, as shown in Fig. 3a and c. For *TIPSAntPT*, by contrast, the bulky phenyl groups prevented the conjugated cores of the *TIPSAntPT* molecules in one column from adjoining the two *TIPS* groups in an adjacent column. As a result, the conjugated cores of *TIPSAntPT* molecules in one column adjoined the conjugated cores of molecules in

Table 2
Electrochemical properties of the small molecules.

	E_{ox} (mV)[a]	E_{red} (mV)[a]	HOMO (eV)[b]	LUMO (eV)[b]	E_g (eV)	E_{g_opt} (eV) [c]
TIPSAntT	990	−1680	−5.39	−2.72	2.67	2.38
TIPSAntBeT	1130	−1310	−5.53	−3.09	2.44	2.36
TIPSAntPT	960	−1440	−5.36	−2.97	2.39	2.18

[a] E_{ox}, and E_{red} stand for the oxidation potential and the reduction potential, respectively.
[b] HOMO = $-(E_{ox} + 4.4)$ eV, LUMO = $-(E_{red} + 4.4)$ eV.
[c] Optical bandgap derived from UV–vis onset.

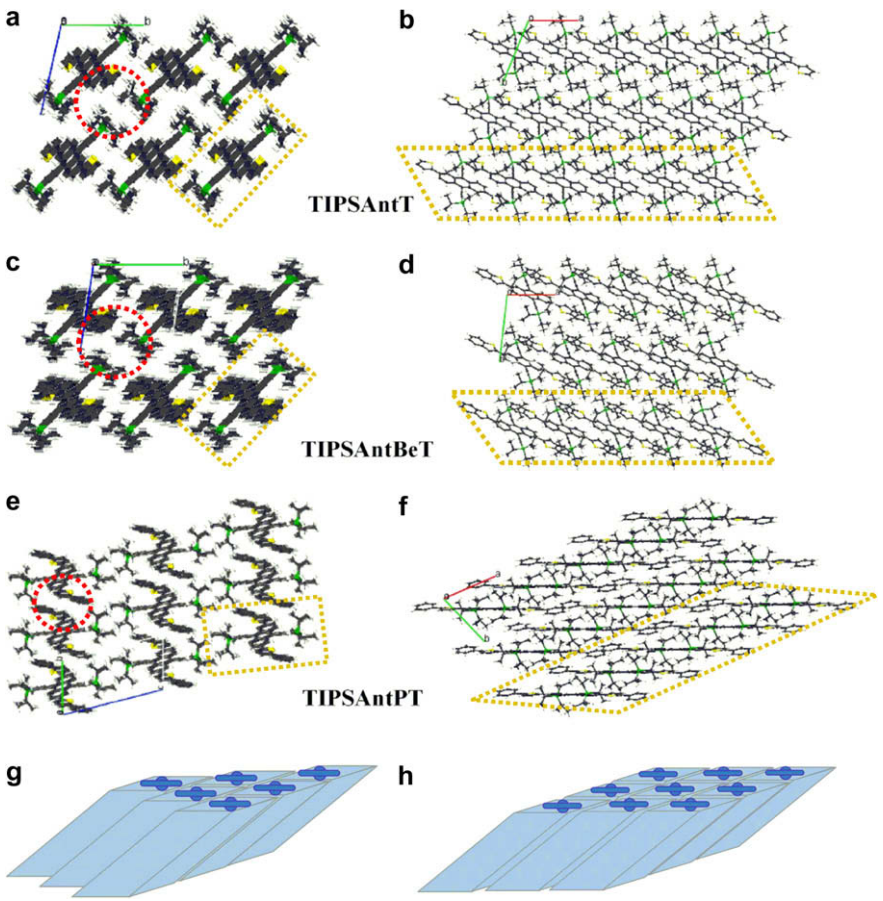

Fig. 3. Single crystal structures of (a and b) *TIPSAntT* and (c and d) *TIPSAntBeT*, which show "slipped-stacked" structures, and (e and f) *TIPSAntPT*, which shows a "bricklayer" structure. (a, c and e): view down crystallographic *a* axis, (b, d, and f): view down crystallographic *c* axis. Schematic figures of columns of *TIPSAnts* stacks: (g) for *TIPSAntT* and *TIPSAntBeT*, and (h) for *TIPSAntPT*. Yellow dotted squares indicate columns of *TIPSAnts* stack and red dotted circles indicate adjoining areas between adjacent columns. (For interpretation of the references to colour in this figure legend, the reader is referred to the web version of this article.)

adjacent columns, resulting in a "bricklayer" structure, as shown in Fig. 3e. *TIPSAntPT* is the first *TIPSAnt* derivative to yield a "bricklayer" stacking structure. In Fig. 3g and h, the *TIPSAnt* columns and the adjoining areas between adjacent columns are indicated by yellow and red dotted lines, respectively.

Fig. 4 shows the area of π-overlap between a molecule and above adjacent molecules of *TIPSAnt* derivatives. (The area of π-overlap with below adjacent molecules was omitted for clarity.) When bulkier substituents were incorporated into the conjugated core, the area of π-overlap increased. As a result, *TIPSAntBeT* had a larger π-overlap area than *TIPSAntT*. Only *TIPSAntPT* showed an additional area of π-overlap with adjacent molecules due to the "bricklayer" stacking structure. This additional area of π-overlap significantly improved the charge-carrier mobility.

3.6. TFT performances

Top-contact OTFTs were fabricated on a common gate of highly n-doped silicon with a 300 nm thick thermally grown SiO_2 dielectric layer. Substrates were modified with

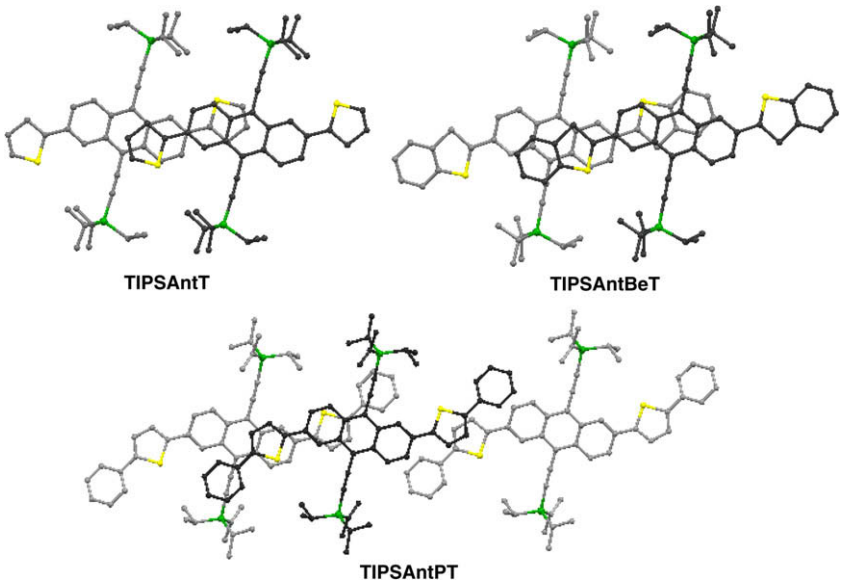

Fig. 4. Overlap of the molecules (dark-shaded molecules) along with their closest neighbors in the plane above the molecule (light-shaded molecules).

octyltrichlorosilane (OTS) by incubation in a toluene solution of OTS for 2 h at room temperature. Films of the organic semiconductors were spin-coated at 2000 rpm from a 0.5 wt.% chloroform solution of *TIPSAntT* and *TIPSAntPT*, and chlorobenzene for *TIPSAntBeT*, due to solubility limitations. All of the TFT results were obtained in ambient air condition and the devices did not show any unstable problems. As shown in Fig. 5, the TFT devices of all molecules showed typical p-channel responses and good saturation behavior. The TFT performances of *TIPSAnts* are summarized in Table 3. *TIPSAntPT* showed the most improved TFT performance among the three molecules, with an average mobility of 0.063 cm^2/Vs, on/off ratio of 4×10^5, and threshold voltage (V_T) of −4.0 V. *TIPSAntPT* showed an order of magnitude larger charge-carrier mobility than *TIPSAntT*, most likely because of the "bricklayer" structure of the film. *TIPSAntBeT*, however, showed a lower mobility than *TIPSAntT*. Although a larger area of π-overlap was observed, as shown in Fig. 4, *TIPSAntBeT* exhibited decreased mobility on account of its poorer solubility and higher crystallinity arising from the rigid benzothiophene. In addition, high crystallinity increased the number of hole-trapping sites at the interface between the OTS monolayer and the *TIPSAntBeT* film. If there were too many hole-trapping sites, a very large negative gate bias would be required to swing the polymer into hole accumulation mode, by inducing a high threshold voltage, V_T. The low HOMO level of *TIPSAntBeT* also produced a hole injection barrier. As a result, V_T of *TIPSAntBeT* (−28.7 V) was much larger than V_T for the other small molecules. The trend in TFT performance among the three small molecules corresponded with the morphological properties, which are discussed in the next section.

Single crystal TFTs based on the small molecules were fabricated because single organic crystals allow the facile investigation of the intrinsic material parameters that determine charge transport efficiency [25,26]. In particular, single crystals of functionalized pentacene reportedly yielded high mobilities because they were largely free from grain boundaries and molecular disorder, and, thus, overlap of the π-orbitals was enhanced [27]. A saturated chlorobenzene solution of the small molecules was slowly evaporated at room temperature onto OTS-modified SiO_2 substrates. After 1 or 2 days, well-defined rod-type single crystals were obtained, and gold electrodes were patterned onto the single crystals by thermal evaporation. The width and length of the channels were calculated from optical microscopy (OM) images. OM images of single crystal TFTs and a schematic device structure are shown in Fig. 6 The mobility trend for single crystal devices was the same as that of the film devices (*TIPSAntBeT* < *TIPSAntT* < *TIPSAntPT*). As expected, the highest TFT performances, showing a mobility of 0.12 cm^2/Vs, were achieved from one-dimensional (1D) single crystalline *TIPSAntPT* microribbons. The improved performance arose from the highly efficient π-orbital overlap of the "bricklayer" structure of the *TIPSAntPT* single crystals. *TIPSAntT* also grew as 1D single crystalline microribbons, resulting in a high mobility, but the less efficient π-orbital overlap of the "slipped-stacked" arrangement of *TIPSAntT* single crystals resulted in a lower mobility than was observed for *TIPSAntPT* single crystals. In contrast, *TIPSAntBeT* grew as three-dimensional (3D) polyhedron single crystals with a larger thickness than *TIPSAntPT*. (The thickness of single crystals was 80 and 200 nm for *TIPSAntPT* and *TIPSAntBeT*, respectively, measured with an Alpha Step 400, Tencor.) In single crystal TFTs, 1D or 2D microrods showed much higher TFT performance than 3D polyhedra because 3D polyhedra have difficulties contacting the gold electrodes [28,29]. As a result, the mobility of *TIPSAntBeT* single crystals was poor. TFT results of single crystals of the *TIPSAnt* derivatives are summarized in Table 3. We are currently working on improving device performances including operational stability and we will publish the results elsewhere.

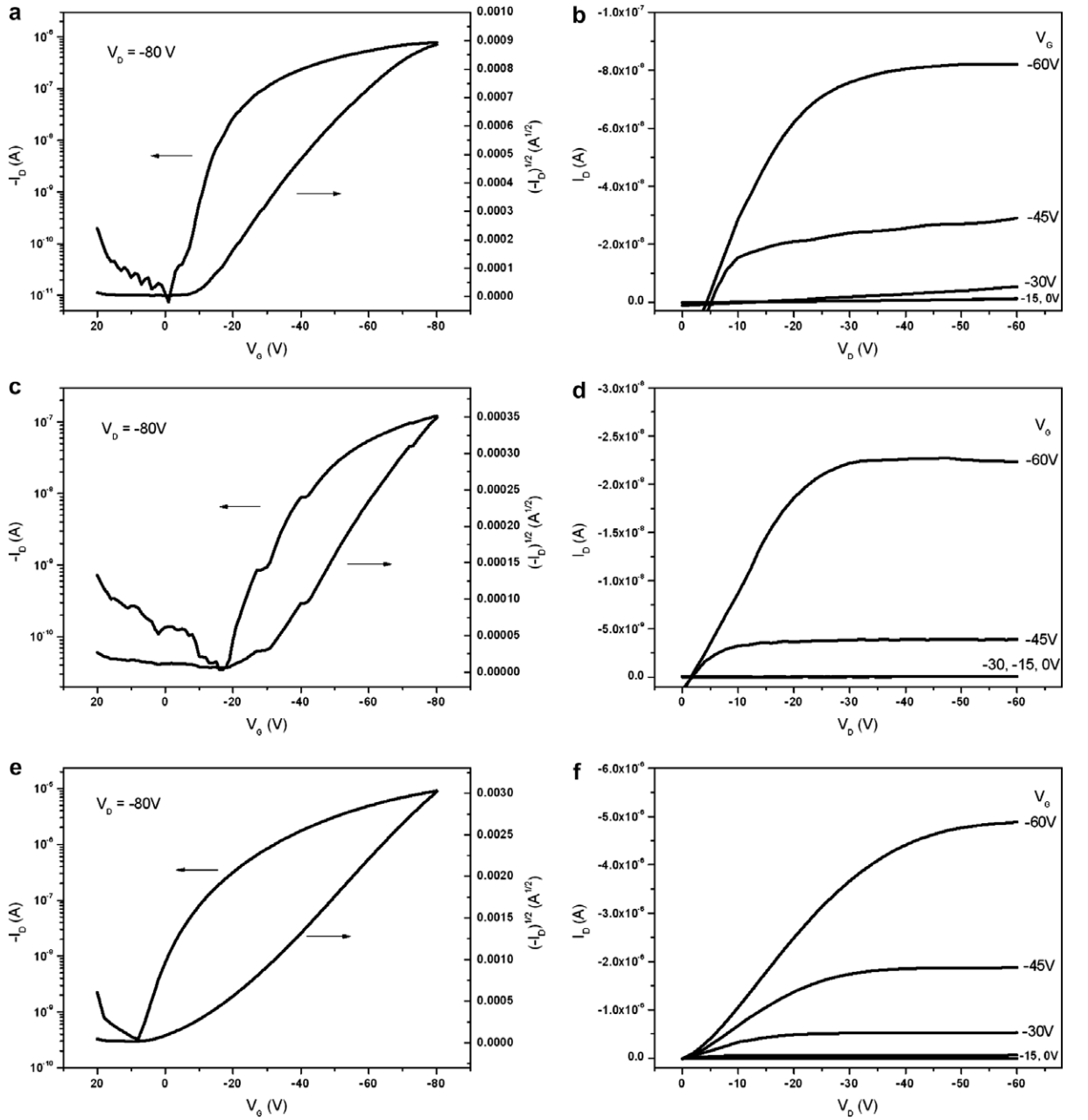

Fig. 5. Transfer characteristics and output characteristics of *TIPSAntT* (a and b), *TIPSAntBeT* (c and d), and *TIPSAntPT* (e and f).

3.7. Morphological properties

We performed atomic force microscopy (AFM) measurements to further investigate the relationship between molecular alignment in films and device performance as AFM provides the thin-film morphologies in micrometer scales to hundreds of nanometer scales. As shown in Fig. 7c, *TIPSAntPT* showed film morphologies dominated by 2D growth after spin-casting, due to the strong electronic interactions in the "bricklayer" π-stacking structure. Each crystalline domain connected smoothly in the as-cast film, yielding devices with high TFT hole mobilities based on *TIPSAntPT*. In contrast, *TIPSAntT* and *TIPSAntBeT* underwent 3D film growth, as shown in Fig. 7a and b, due to the limited π-overlap in the "slipped-stacked" structures. *TIPSAntBeT*, especially, showed poor substrate coverage, with the needle-like crystallites produced due to poor solubility. The high crystallinity also led to a very low mobility and high V_T. The rotational invariance of the fused benzothiophene in the backbone facilitated the adoption of a low energy backbone conformation, promoting the formation of highly ordered crystalline domains.

Out-of-plane and in-plane mode X-ray diffraction (XRD) spectra of films of the molecules were measured,

Table 3
TFT performances of the small molecules.

	Film			Single crystal		
	Mobility (cm^2/Vs)	I_{on}/I_{off}	V_T (V)	Mobility (cm^2/Vs)	I_{on}/I_{off}	V_T (V)
TIPSAntT	0.0039	6×10^4	−11.2	0.059	5×10^3	−24.1
TIPSAntBeT	0.0013	7×10^3	−28.7	0.0067	3×10	−8.5
TIPSAntPT	0.063	4×10^5	−4.0	0.12	2×10^2	−6.1

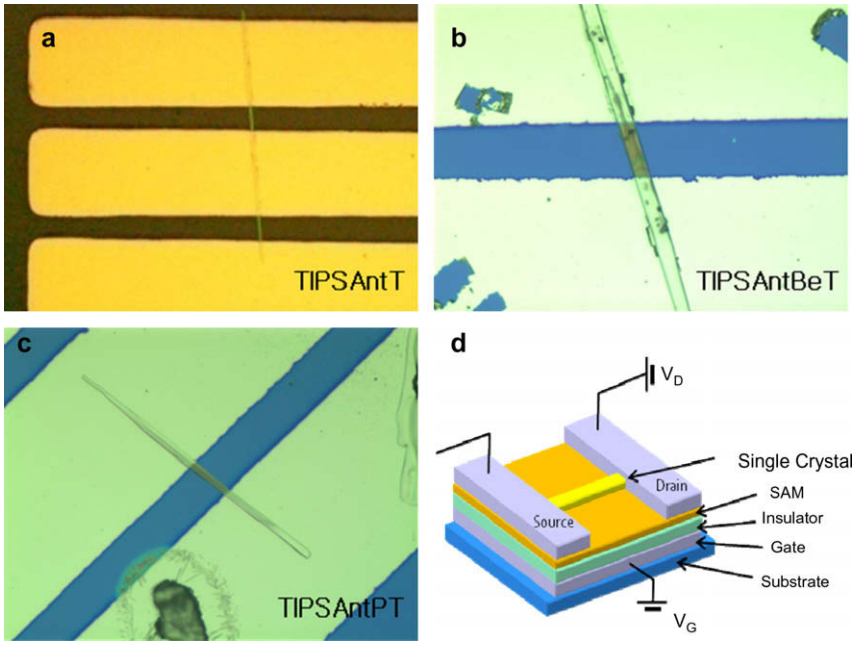

Fig. 6. Optical microscopy images of single crystal TFTs of (a) *TIPSAntT*, (b) *TIPSAntBeT*, and (c) *TIPSAntPT*. (d) Schematic device structure of single crystal TFTs.

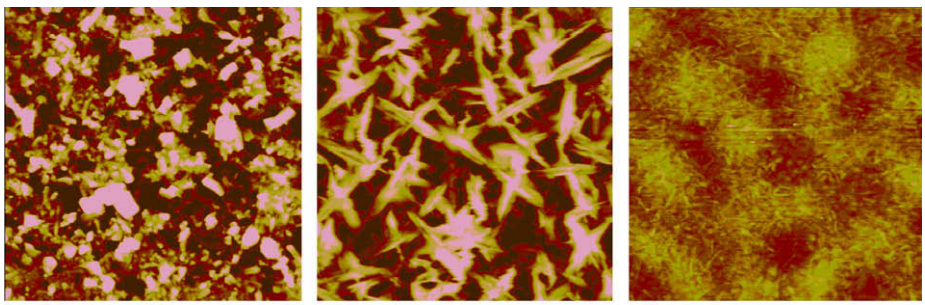

Fig. 7. AFM images (5μ × 5μ).

as shown in Fig. 8. The *TIPSAntT* film showed the lowest degree of crystallinity, exhibiting no specific ordering in the peaks of the out-of-plane mode XRD. Although a (0 1 0) peak was observed in the in-plane mode XRD of the *TIPSAntT* film, the interlayer spacing *d* was 4.28 Å, which is the largest spacing measured among the three molecules, indicating less effective intermolecular π-stacking. In contrast, *TIPSAntBeT* films showed highly crystalline properties, with (1 0 0), (2 0 0), and (3 0 0) reflections in the out-of-plane mode XRD indicating well-organized intraplanar lamella-like structures oriented normal to the substrate. The molecular length of the *TIPSAnt* derivatives along the *TIPS* axis was 16.7 Å, as determined by X-ray crystallography. The *d* spacing of the (1 0 0) peak was 14.9 Å, which implied that *TIPSAntBeT* molecules were aligned perpendicular to the substrate, with respect to

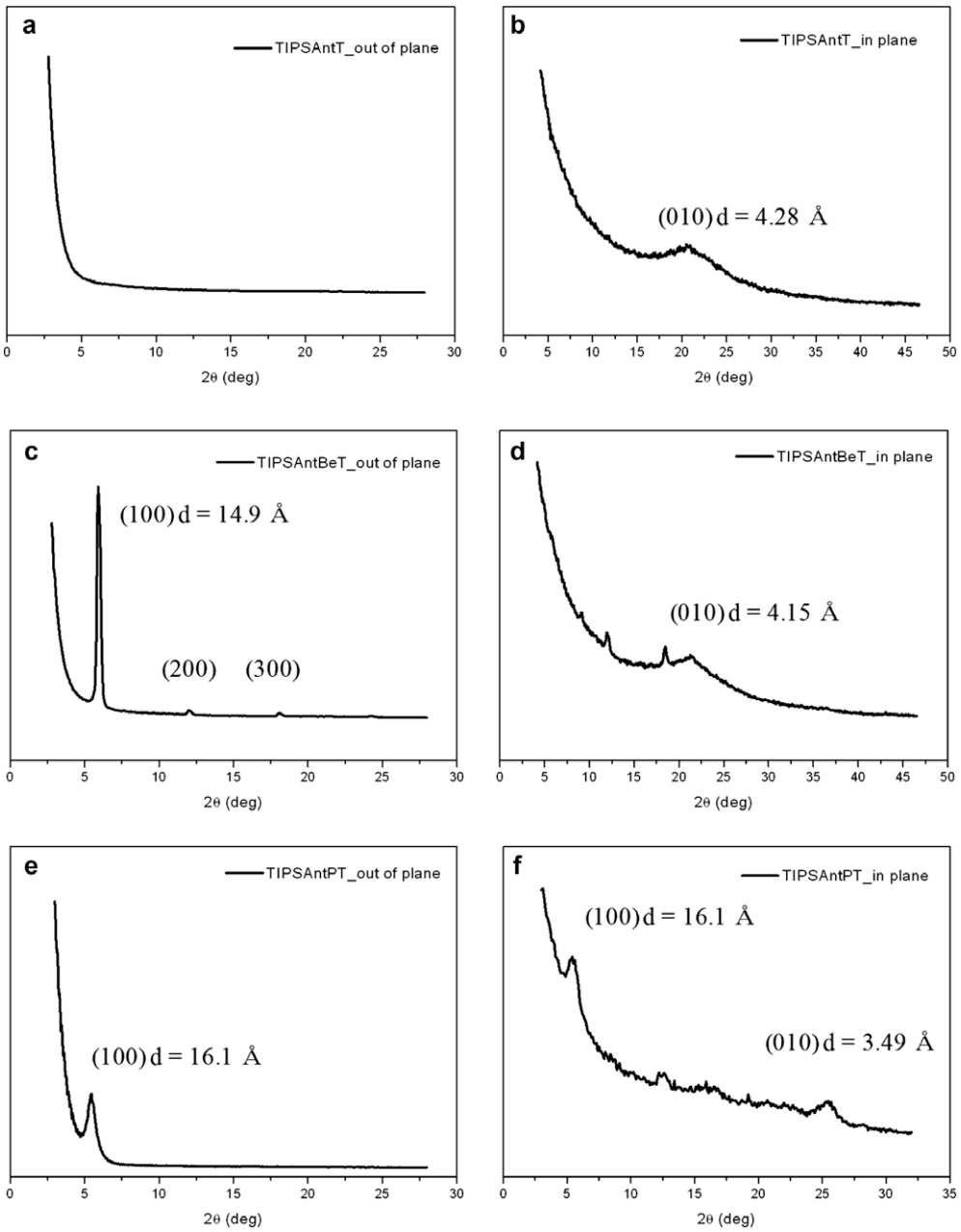

Fig. 8. XRD patterns (a) *TIPSAntT*_out of plane, (b) *TIPSAntT*_in-plane, (c) *TIPSAntBeT*_out of plane, (d) *TIPSAntBeT*_in-plane, (e) *TIPSAntPT*_out of plane, and (f) *TIPSAntPT*_in-plane.

the *TIPS* axis, with a tilt angle of 27°. Although the (0 1 0) peak in the in-plane mode XRD of the *TIPSAntBeT* films showed a closer interlayer *d* spacing of 4.15 Å, the high crystallinity of the *TIPSAntBeT* films resulted in poorer device performances than *TIPSAntT*. The high crystallinity of the *TIPSAntBeT* probably arose from a π-overlap area that was larger than that of *TIPSAntT*, as expected from X-ray crystallography. *TIPSAntPT* films showed the most promising XRD results in both out-of-plane and in-plane mode XRD experiments. The *d* spacing of the (1 0 0) peak was 16.1 Å, implying that *TIPSAntPT* was aligned more perpendicularly to the substrate along the *TIPS* axis than was *TIPSAntBeT*, with a smaller tilt angle of 15°. When the molecules were aligned perpendicular to the substrate, the π-overlap between adjacent molecules was maximized, and carrier transport could occur more effectively. In-plane XRD of *TIPSAntPT* showed a (0 1 0) peak that indicated the interlayer *d* spacing of 3.49 Å. This value was very close to the interplanar distances (3.54 Å) determined by X-ray crystallography measurements, indicating highly effective π-orbital overlap due to the "bricklayer" structure.

4. Conclusions

We synthesized three new *TIPSAnt* derivatives and carried out comparative studies among these three molecules to investigate the relationship between the molecular structures and TFT performances. Only *TIPSAntPT* showed a "bricklayer" stacking structure that resulted in a high charge-carrier mobility of 0.063 cm^2/Vs in the film state and 0.12 cm^2/Vs in the single crystal state. This result agreed well with the AFM and XRD findings. Although the rigidity of the substituents and large area of π-overlap resulted in high crystallinity for the *TIPSAntBeT*, the lack of solubility and the needle-like crystalline films reduced the device performance. These results provide valuable insight into the design of new small molecules for solution-processable OTFTs.

Acknowledgements

This research was supported by a grant (F0004011-2008-31) from the Information Display R&D Center, one of the 21st century Frontier R&D Programs funded by the Ministry of Commerce, Industry, and Energy of the Korean Government. We gratefully acknowledge Dr. J.-H. Kim and Dr. S.K. Lee for assistance with XRC measurements.

References

[1] A.R. Murphy, J.M.J. Frechet, Chem. Rev. 107 (2007) 1066.
[2] H.E. Katz, Chem. Mater. 16 (2004) 4748.
[3] B.S. Ong, Y.L. Wu, Y.N. Li, P. Liu, H.L. Pan, Chem. Eur. J. 14 (2008) 4766.
[4] S. Allard, M. Forster, B. Souharce, H. Thiem, U. Scherf, Angew. Chem. Int. Ed. 47 (2008) 4070.
[5] A.R. Murphy, J.M.J. Frechet, P. Chang, J. Lee, V. Subramanian, J. Am. Chem. Soc. 126 (2004) 1596.
[6] H. Sirringhaus, Adv. Mater. 17 (2005) 2411.
[7] M.M. Payne, S.R. Parkin, J.E. Anthony, C.C. Kuo, T.N. Jackson, J. Am. Chem. Soc. 127 (2005) 4986.
[8] K.C. Dickey, J.E. Anthony, Y.L. Loo, Adv. Mater. 18 (2006) 1721.
[9] J.E. Anthony, D.L. Eaton, S.R. Parkin, Org. Lett. 4 (2002) 15.
[10] S. Subramanian, S.K. Park, S.R. Parkin, V. Podzorov, T.N. Jackson, J.E. Anthony, J. Am. Chem. Soc. 130 (2008) 2706.
[11] M.L. Tang, A.D. Reichardt, T. Siegrist, S.C.B. Mannsfeld, Z.N. Bao, Chem. Mater. 20 (2008) 4669.
[12] M.L. Tang, A.D. Reichardt, N. Miyaki, R.M. Stoltenberg, Z. Bao, J. Am. Chem. Soc. 130 (2008) 6064.
[13] J.H. Park, D.S. Chung, J.W. Park, T. Ahn, H. Kong, Y.K. Jung, J. Lee, M.H. Yi, C.E. Park, S.K. Kwon, H.K. Shim, Org. Lett. 9 (2007) 2573.
[14] K. Fukui, C. Nagata, T. Yonezawa, K. Morokuma, Bull. Chem. Soc. Jap. 34 (1961) 230.
[15] M. Manoharan, F.D. Proft, P. Geerlings, J. Chem. Soc. Perkin Trans. 2 (2000) 1767.
[16] K.H. Jung, S.Y. Bae, K.H. Kim, M.J. Cho, K. Lee, Z.H. Kim, D.H. Choi, D.H. Lee, D.S. Chung, C.E. Park, Chem. Commun. (2009) 5290.
[17] D.S. Chung, J.W. Park, J.H. Park, G.H. Kim, H.S. Lee, D.H. Lee, H.K. Shim, S.K. Kwon, C.E. Park, J. Mater. Chem. 20 (2010) 524.
[18] Y. Dienes, S. Durben, T. Karpati, T. Neumann, U. Englert, L. Nyulaszi, T. Baumgartner, Chem. Eur. J. 13 (2007) 7487.
[19] A.J. Sandee, C.K. Williams, N.R. Evans, J.E. Davies, C.E. Boothby, A. Kohler, R.H. Friend, A.B. Holmes, J. Am. Chem. Soc. 126 (2004) 7041.
[20] J.J. Li, K.G. Carson, B.K. Trivedi, W.S. Yue, Q. Ye, R.A. Glynn, S.R. Miller, D.T. Connor, B.D. Roth, J.R. Luly, J.E. Low, D.J. Heilig, W.X. Yang, S.X. Qin, S. Hunt, Bioorg. Med. Chem. 11 (2003) 3777.
[21] C.R. Swartz, S.R. Parkin, J.E. Bullock, J.E. Anthony, A.C. Mayer, G.G. Malliaras, Org. Lett. 7 (2005) 3163.
[22] R. Cervini, X.C. Li, G.W.C. Spencer, A.B. Holmes, S.C. Moratti, R.H. Friend, Synth. Met. 84 (1997) 359.
[23] I. Mcculloch, M. Heeney, C. Bailey, K. Genevicius, I. Macdonald, M. Shkunov, D. Sparrowe, S. Tierney, R. Wagner, W.M. Zhang, M.L. Chabinyc, R.J. Kline, M.D. Mcgehee, M.F. Toney, Nat. Mater. 5 (2006) 328.
[24] H. Meng, J. Zheng, A.J. Lovinger, B.C. Wang, P.G. Van Patten, Z.N. Bao, Chem. Mater. 15 (2003) 1778.
[25] V. Podzorov, E. Menard, A. Borissov, V. Kiryukhin, J.A. Rogers, M.E. Gershenson, Phys. Rev. Lett. 93 (2004) 86602.
[26] J.Y. Lee, S. Roth, Y.W. Park, Appl. Phys. Lett. 88 (2006) 252106.
[27] V. Podzorov, S.E. Sysoev, E. Loginova, V.M. Pudalov, M.E. Gershenson, Appl. Phys. Lett. 83 (2003) 3504.
[28] J.A. Lim, H.S. Lee, W.H. Lee, K. Cho, Adv. Funct. Mater. 19 (2009) 1515.
[29] C.L. Wang, Y.L. Liu, Z.Y. Ji, E.J. Wang, R.J. Li, H. Jiang, Q.X. Tang, H.X. Li, W.P. Hu, Chem. Mater. 21 (2009) 2840.